Journal of Luminescence 289 (2026) 121631

Contents lists available at ScienceDirect

Journal of Luminescence

journal homepage: www.elsevier.com/locate/jlumin

Full Length Article

Identification of defect centers responsible for TL in fluorapophyllite crystal using EPR and optical absorption techniques

Reinaldo de Melo Ferreira [a], Nilo F. Cano [b,*], Betzabel N. Silva-Carrera [a], T.K. Gundu Rao [c], J.F. Benavente [d], Edwar A. Canaza [c], Jessica Mosqueira-Yauri [c], René R. Rocca [b], J.F.D. Chubaci [a,e]

[a] Instituto de Pesquisas Energéticas e Nucleares, IPEN-CNEN/SP, São Paulo, SP, Brazil
[b] Universidade Federal de São Paulo, Instituto do Mar, SP, Brazil
[c] Universidad Nacional de San Agustín de Arequipa - UNSA, Arequipa, Peru
[d] CIEMAT, Av. Complutense 40 E, 28040, Madrid, Spain
[e] Universidade de São Paulo, Instituto de Física, São Paulo, SP, Brazil

ARTICLE INFO

Keywords:
Fluorapophyllite
TL glow curve
Optical absorption
EPR
Effect of heat treatment and gamma irradiation

ABSTRACT

In this work, the natural fluorapophyllite crystal ($KCa_4Si_8O_{20}(F,OH)\cdot 8(H_2O)$) has been studied by techniques such as X-ray diffraction (XRD), X-ray fluorescence (XRF), scanning electron microscopy (SEM), energy dispersive spectroscopy (EDS), thermoluminescence (TL), optical absorption (OA), and electron paramagnetic resonance (EPR). This crystal, sensitized by heat treatment at 700 °C, has four TL peaks which, when superimposed, give rise to a broad peak centered at 225 °C, and an emission band between 300 and 600 nm centered at 475 nm. The kinetic parameters of the TL peaks were determined using the Tm-Tstop and deconvolution methods. In addition, a statistical analysis of the deconvolution residue was performed to evaluate the accuracy of the deconvolution. Electron paramagnetic resonance (EPR) analysis identified the defect centers induced in the crystal by gamma radiation: a center due to V^{4+}, and a center associated with oxygen (O^- ion). The V^{4+} center is interpreted as a (VO^{2+}) radical ($g \approx 1.967$). The O^- center is characterized by axial symmetry, and the center relates to the TL peaks from 230 to 306 °C.

1. Introduction

Silicates are the most abundant group of minerals in the Earth's crust, constituting more than 95 % of its volume and acting as essential components in the formation of rocks [1]. These minerals are of great economic and technological relevance and are used in industrial sectors, high technology, gemology, and fundamental research in the fields of geology, chemistry, and physics. During the genesis of these materials, many elements foreign to their fundamental structure are incorporated, which are called impurities. Within the predominantly ionic crystal structure of silicates, impurities and thermodynamic imperfections of the crystal lattice itself play a fundamental role in defining peculiar physical properties with numerous practical applications, especially significant in radiation dosimetry [2–4]. Originally, apophyllite was classified as a single mineral [5], characterized by a variable fluorine-hydroxyl composition. However, in 1978, the International Mineralogical Association (IMA) proposed a revision of this classification, subdividing the mineral species into two distinct ones: fluorapophyllite and hydroxyapophyllite [6]. Later, in 1981, a third rare species, natroapophyllite, was identified, characterized by the substitution of potassium for sodium in its crystal structure [7]. More recently, to standardize mineralogical nomenclature and facilitate cataloging and alphabetical indexing, the IMA revised the names of these species [8]. The new names are apophyllite-(KF) (previously fluorapophyllite), apophyllite-(KOH) (previously hydroxyapophyllite), and apophyllite-(NaF) (previously natroapophyllite).

Fluorapophyllite, chemical formula $KCa_4Si_8O_{20}(F,OH)\cdot 8(H_2O)$, is a mineral belonging to the phyllosilicate group and corresponds to a hydrated fluorosilicate of calcium and potassium [6]. It crystallizes in the tetragonal system, often presenting well-formed prismatic crystals with characteristic pyramidal terminations [9]. Its structure shows excellent cleavage in one direction, giving rise to lamellar fragments, and the

* Corresponding author.
E-mail addresses: nilocano@if.usp.br, nilo.cano@unifesp.br (N.F. Cano).

https://doi.org/10.1016/j.jlumin.2025.121631
Received 15 August 2025; Received in revised form 3 October 2025; Accepted 26 October 2025
Available online 27 October 2025

crystals generally have a glassy to pearly luster, with colors ranging from colorless, white, pale green, light yellow, and light pink. Its tetragonal crystal lattice has typical *P*4/mnc space group parameters, z = 2, a = 8.976 nm, and c = 15.792 nm at 295 K [10]. This mineral is widely found in cavities of volcanic rocks, mainly basaltic, and is highly appreciated by collectors due to the beauty and sharpness of its crystals. Fluorapophyllite is a low-temperature mineral that is usually found filling cavities or veins in basic alkaline and calcareous rocks. In these environments, it is usually associated mainly with minerals of the zeolite group [11]. Although it is not a zeolite, part of the water is considered zeolitic as it is trapped between the layers of the mineral, and another part is bound to the crystalline structure itself [12].

Luminescent materials, whether natural or synthetic, are widely used in radiation dosimetry and archaeological and geological dating. The defect centers created by ionizing radiation are responsible for the luminescence of the material. The identification and characterization of these centers is an essential step in elucidating the mechanism responsible for the luminescent emission [13–15]. Apophyllite can exhibit luminescent properties under certain conditions. However, this characteristic can vary depending on the specific chemical composition, purity, heat treatment, trace impurities present, and the geological origin of the material, and it can show fluorescence, mainly under short-wave UV radiation, exhibiting colors such as bluish or greenish, although this response is not universal and can vary depending on the impurities present in the sample [16]. These results suggest the potential use of this material in thermoluminescence (TL) and electron paramagnetic resonance (EPR) dosimetry. However, to date, no work has been published specifically addressing the TL and EPR properties of this crystal. Therefore, this study aims to investigate the nature of the luminescence and paramagnetic centers in natural fluorapophyllite and their correlations, analyzing the effects of gamma irradiation and heat treatment by both TL and EPR techniques, to better understand its physical properties and explore possible applications of this crystalline material in the area of ionizing radiation dosimetry.

2. Materials and methods

The fluorapophyllite crystal with chemical formula $KCa_4Si_8O_{20}(F,OH)\cdot 8(H_2O)$ used in this study comes from the state of Rio Grande do Sul, Brazil, and was acquired from the mining and marketing company LEGEP. For TL and EPR measurements, part of the crystals were crushed and sieved, selecting grains with diameters between 0.080 and 0.180 mm. Grains with a diameter less than 0.080 mm were used for X-ray fluorescence (XRF) and X-ray diffraction (XRD) analyses.

The chemical analysis by XRF was carried out on a pressed sample of fluorapophyllite powder in calibration with STD-1 (Standardless), using a Bruker XRF spectrometer model S8 Tiger. Powder XRD measurements were performed on a Rigaku diffractometer model Miniflex 600. The XRD measurements were taken at the interval of Bragg angle 2θ ($10^\circ \leq 2\theta \leq 80^\circ$) with 0.005° step size and speed 4°/min at room temperature.

The morphological analysis of the fluorapophyllite sample after the sensitization process was performed using a Jeol model JSM-IT700HR scanning electron microscope (SEM) coupled to energy dispersive spectroscopy (EDS), which allows qualitative determination of the distribution and homogeneity of the constituent elements of the sample.

A Varian Cary model 7000 spectrophotometer was used for the analysis of the optical properties of fluorapophyllite in the spectral range from 250 to 2500 nm.

EPR experiments were carried out on a Miniscope spectrometer operating in the X-band. Samples, with a mass of 150 mg, were placed in quartz capillary tubes with an internal diameter of 4 mm. EPR spectrum measurements were performed on a fluorapophyllite powder sample, using the following experimental conditions: (i) natural sample not irradiated and (ii) natural sample irradiated with 1 kGy and subjected to different heat treatments between 230 °C and 900 °C. The parameters adopted for the EPR measurements were as follows: microwave frequency in the X-band, modulation frequency of 100 kHz, modulation amplitude of 0.06 mT, and microwave power of 20 mW. The magnetic field was calibrated using 2.2-diphenyl-1-picrylhydrazyl (DPPH), and measurements were performed at room temperature (~20 °C).

TL measurements were performed using a Harshaw model 4500 TL reader in a nitrogen atmosphere; the heating rate was maintained at 5 °C/s. For all TL measurements, aliquots with a mass of 50 mg in powder form with grain sizes between 0.080 and 0.180 mm in diameter were used. Luminescence was detected using a Hamamatsu R647 photomultiplier tube through a Schott KG1 filter, with a transmission band between 330 and 690 nm. Each TL glow curve is the average of five readings using aliquots of samples irradiated with the same dose.

The TL emission spectra were measured by connecting a monochromator in front of the Risø TL/OSL reader detection system. For each wavelength previously selected with the monochromator, the TL glow curve of the sample previously irradiated with a dose of 1 kGy was recorded, with a step size of 10 nm.

The irradiation of powder samples for TL and EPR measurements was carried out using a ^{60}Co gamma source with a dose rate of 379.43 Gy/h at room temperature.

The kinetic parameters, namely, the activation energy (E), the distribution width (σ), the peak intensity of each component (I_M), and the temperature corresponding to the maximum intensity (T_M), were obtained by deconvolution analysis of the TL glow curves acquired at a constant rate of 5 °C/s after irradiation with increasing doses ranging from 50 Gy to 3 kGy. The analysis was carried out using a mathematical model consistent with the Tm-Tstop approach, which assumes that the TL glow curves can be described as a linear combination of four components governed by first-order kinetics (FOK).

$$I_n(T_j) = \sum_{i=1}^{4} {}^{i}F\left(E_i, {}^{i}T_M, {}^{i}I_M, \sigma_i; T_j\right) \tag{1}$$

where ${}^{i}F$ functions are expressed as follow:

$${}^{i}F(T) = I_M \frac{\int_{E_1}^{E_2} f(E)\cdot e^{-\frac{E}{k\cdot T}}\cdot e^{\left\{-\frac{E_0}{k\cdot T_M}\cdot e^{\frac{E_0}{k\cdot T_M}}\cdot\int_{T_0}^{T} e^{-\frac{E}{k\cdot T'}}\cdot dT'\right\}}\cdot dE}{\int_{E_1}^{E_2} f(E)\cdot e^{-\frac{E}{k\cdot T_M}}\cdot e^{\left\{-\frac{E_0}{k\cdot T_M}\cdot e^{\frac{E_0}{k\cdot T_M}}\cdot\int_{T_0}^{T_M} e^{-\frac{E}{k\cdot T'}}\cdot dT'\right\}}\cdot dE} \tag{2}$$

where f(E) are functions that describe the density of trapped charges associated with the energy E. In the case of continuous trap distribution, this function can be written by a Gaussian expression [17]:

$$f(E) = \frac{1}{\sqrt{2\cdot\pi\cdot\sigma^2}} e^{-(E-E_0)^2/2\sigma^2} \tag{3}$$

The deconvolution fitting was performed using version 0.0.2 of the Python CGCD library, developed by J.F. Benavente and J.E. Tenopala. This library implements a least-squares numerical fitting procedure based on an iterative Levenberg-Marquardt algorithm.

3. Results and discussion

Initially, an XRF chemical analysis of the fluorapophyllite sample was carried out, the results of which are shown in Table 1. Comparing the composition obtained ($KCa_4Si_8O_{20}(F,OH)\cdot 8(H_2O)$) with data from a

Table 1
Main oxide components in (weight%) of fluorapophyllite crystal.

Sample	Compound (wt%)					
Fluorapophyllite	SiO_2	CaO	K_2O	F	Na_2O	CoO
	50.6	24.3	5.24	2.12	0.046	0.013

previous study [9], the absence of water was attributed to an ignition loss of 17.6 %, intrinsic to the analytical method used.

Fig. 1 shows the X-ray diffractogram of the powdered fluorapophyllite sample. The XRD data of the sample were compared with the records of the COD (Crystallography Open Database) database. The result, illustrated in Fig. 1, confirmed the identification of the sample as fluorapophyllite, according to the COD file number 9000254. Due to the presence of low-intensity diffraction peaks in the XRD diffractogram, the XRD data were analyzed using the Rietveld refinement method. This analysis was performed using X'Pert HighScore Plus software. The results show the presence of two crystalline phases: 97.9 % fluorapophyllite in its tetragonal phase, with space group *P*4/mnc, and 2.1 % quartz in its trigonal phase. The unit cell of the tetragonal phase of fluorapophyllite, generated with the VESTA program from the lattice parameters obtained from the Rietveld refinement, is shown in the inset of Fig. 1.

Fig. 2 shows an image of the fluorapophyllite sample obtained by SEM and magnified 10000 times. This result shows that the surfaces of the fluorapophyllite particles are irregular and present incrustations of smaller particles. In addition, the cleavage planes of the crystal are observed. Elemental mapping profiles (Fig. 2(b) to 2(e)) and EDS spectra (Fig. 2(f)) of one of the fluorapophyllite particles confirm the presence of K, Ca, Si, and O uniformly distributed in the crystal. In addition, the elemental analysis by EDS confirms the results obtained by the XRF technique.

The optical absorption (OA) analysis of the natural fluorapophyllite sample was performed in order to identify the presence of water molecules within the crystal structure, corroborating previous studies and justifying the anomalies observed in the analyses of the TL glow curves observed in this work. Fig. 3 shows the OA spectrum of the fluorapophyllite sample, revealing the presence of three main spectral regions: (i) between 1200 and 1600 nm, due to overlapping vibrations of hydroxyl and water molecules (with absorption at 1442 nm, characterizing weakly hydrogen-bonded water molecules); (ii) between 1800 and 2100 nm, a band associated with weakly surface-bound water

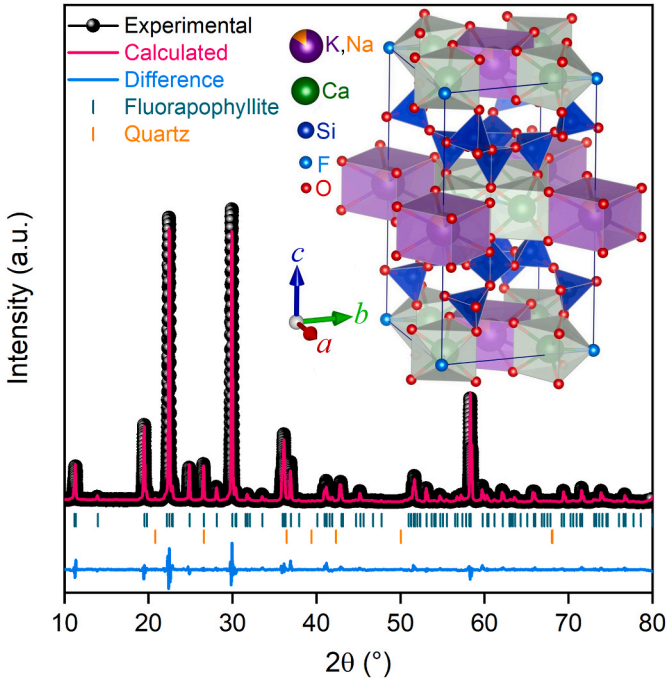

Fig. 1. XRD patterns of the fluorapophyllite sample. Experimental (black full circle), calculated (pink solid line) and residual (light blue solid line). The rows of vertical lines give the positions of all possible Bragg reflections for fluorapophyllite (green vertical line), COD 9000254, and quartz (orange vertical line), COD 9005019. COD - Crystallography Open Database.

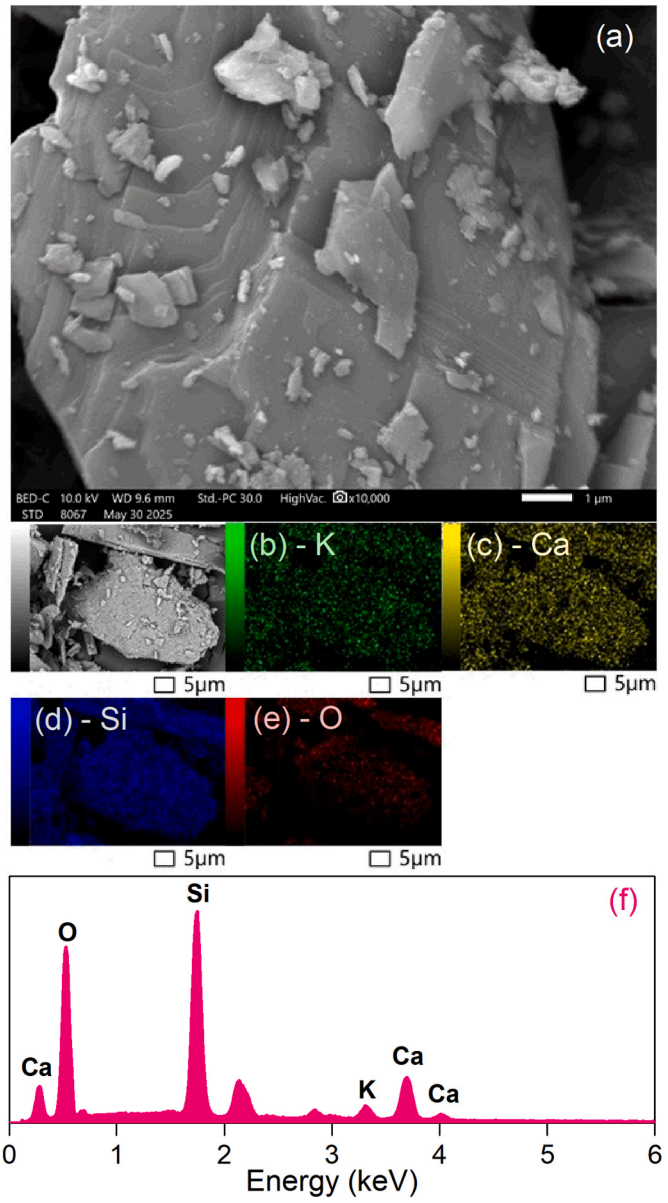

Fig. 2. (a) SEM image at 10000 times magnification of a fluorapophyllite crystal particle after heat treatment at 700 °C. (b–e) Elemental mapping and (h) EDS analysis of a fluorapophyllite crystal particle.

molecules (peak at 1914 nm); and (iii) between 2340 and 2600 nm, corresponding to stretching and deformation of hydroxyl modes [18]. A less intense band was also identified at 1550 nm, attributed to the NH_2 radical; this result indicates the presence of ammonia molecules in the fluorapophyllite sample.

Initially, natural fluorapophyllite samples were subjected to different thermal treatments to remove the natural radiation-induced TL signal from their geological formation and to investigate the sensitization of their TL response to such treatments.

The TL response of samples subjected to a dose of 1 kGy previously heat-treated at different temperatures presented incoherent and almost random signals when subjected to heat treatments below 500 °C; this behavior in their TL response is possibly due to the presence of water molecules within their crystalline structure. However, heat treatments between 500 and 700 °C resulted in more intense, coherent, and reproducible TL glow curves, as shown in Fig. 4. To study the TL emission as a function of radiation dose, the heat treatment at 700 °C was adopted, which provided higher sensitivity and intensity of the TL signal

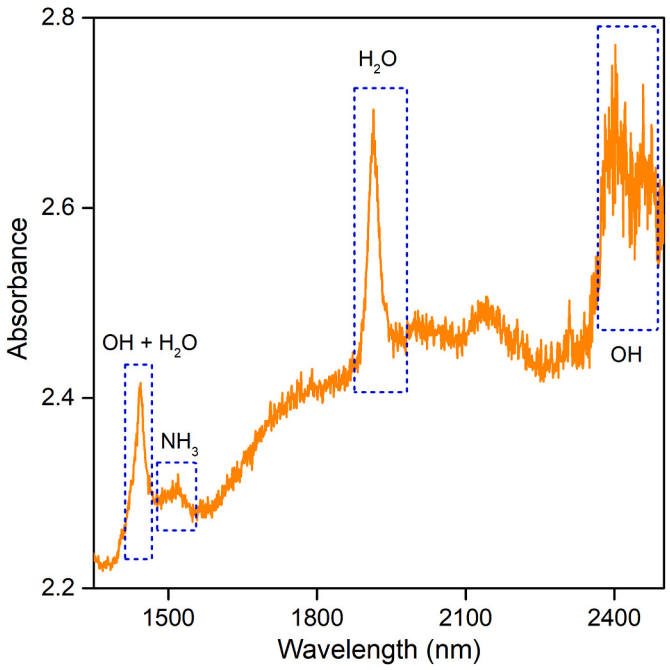

Fig. 3. Optical absorption spectrum of a natural fluorapophyllite sample.

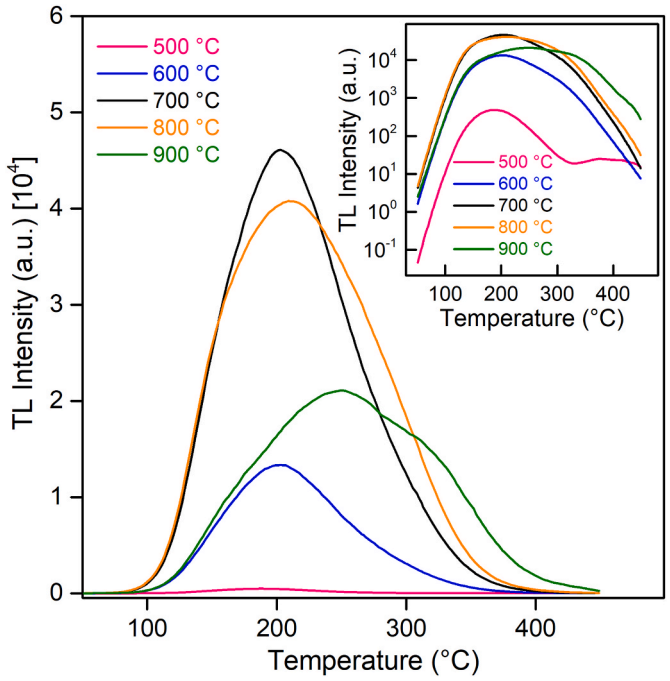

Fig. 4. TL glow curves of natural samples heat-treated from 500 to 900 °C, irradiated with a dose of 1 kGy. The inset of the figure shows the same TL glow curves in a semi-logarithmic scale.

(see Fig. 4), ensuring the complete dehydration of the sample [19,20]. For annealing temperatures above 800 °C, the TL intensity of the glow curve decreases and presents TL peaks around 250 and 320 °C superimposed on the main peak at 230 °C. From these results, a temperature of 700 °C was established as the sensitization temperature of the fluorapophyllite crystal.

Fig. 5(a) shows the TL glow curves of fluorapophyllite samples previously irradiated with gamma radiation doses in the range of 1 Gy–3 kGy. The TL glow curve for all doses shows the superposition of two or

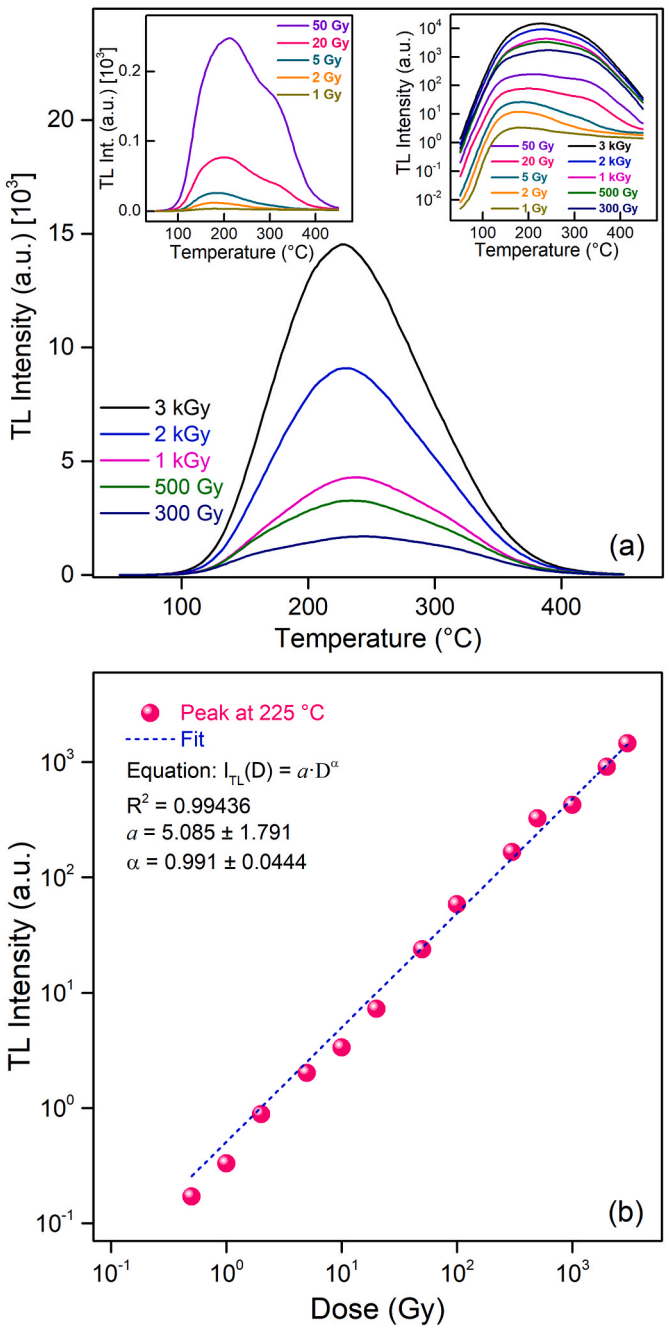

Fig. 5. (a) TL glow curves of fluorapophyllite samples previously heat-treated at 700 °C and irradiated with various doses of gamma. The inset of the figure (right side) shows the same TL glow curves in a semi-logarithmic scale. (b) Behavior of TL intensity as a function of gamma radiation dose. The blue dashed line shows the fit using equation (4).

more peaks giving rise to a broad peak centered at 225 °C for doses between 300 Gy and 3 kGy. For radiation doses in the 1–50 Gy range, the presence of a peak around 310 °C is more evident. The central peak at 225 °C is more intense and grows faster than the peak at 310 °C, as can be seen in the representation of the TL glow curves on a semi-logarithmic scale (see the inset in Fig. 5(a), right side).

The position of the peaks does not vary with the irradiation dose. This means that the maximum peaks (Tm) are independent of the initial carrier concentration [21]. According to Pagonis and Kitis [22], this type of behavior is characteristic of TL peaks that obey first-order kinetics.

Fig. 5(b) shows the linearity analysis of the TL response of the

maximum peak intensity centered at 225 °C for the sample. The linearity coefficient was analyzed using the equation proposed by Halperin and Chen [23]:

$$I_{TL}(D) = a \cdot D^{\alpha} \quad (4)$$

where I_{TL} is the TL intensity, a is a coefficient, D is the dose, and α is the linearity factor, which must be equal to 1 for a linear dependence on the logarithmic scale graph.

The behavior of the peak intensity at 225 °C as a function of dose was fitted with a linear correlation coefficient of 0.991, indicating a linear dependence for the peak at 225 °C, with no saturation for the highest dose range used.

Fig. 6 shows the 2D TL emission spectrum of the fluorapophyllite sample irradiated with a dose of 1 kGy. This result shows that the broad TL peak centered at 225 °C has a main TL emission band at 475 nm.

The TL glow curves of the fluorapophyllite samples are considered to exhibit several TL peaks, superimposed on each other, forming a broad peak centered at 225 °C.

The Tm-Tstop method [24] was applied to the sample previously heat treated at 700 °C and then irradiated with a gamma ray dose of 1 kGy. The results obtained using the Tm-Tstop method reveal a series of overlapping TL components linked to continuous electron trap distributions (see Fig. 7). Furthermore, the invariance of the position of the peaks observed in Fig. 5 shows the presence of TL peaks that obey first-order kinetics (FOK). Also, in Fig. 5, we can see that the peak located at 225 °C showed a significantly higher intensity than the others, which caused their overlapping, giving the appearance of a broad peak.

The mathematical model selected is supported by recent studies [25], which demonstrate that applying kinetic models of order higher than one can introduce substantial systematic errors, particularly under conditions of significant peak overlap. Such errors often lead to notable discrepancies between the fitted and true kinetic parameter values.

To avoid these issues, a first-order kinetics approach was employed, wherein the observed peak broadening is attributed to the width of the trap energy distributions, an interpretation consistent with the outcomes of the Tm-Tstop analysis.

Fig. 8 shows four TL peaks obtained by the deconvolution method using a mathematical model based on first-order kinetics.

The proposed model, consisting of four components governed by first-order kinetics with continuous trap distributions, has been applied to the experimental data. The results of the deconvolution analysis are tabulated in Annex I, while the validity of the implemented mathematical model is assessed through both the statistical analysis of the

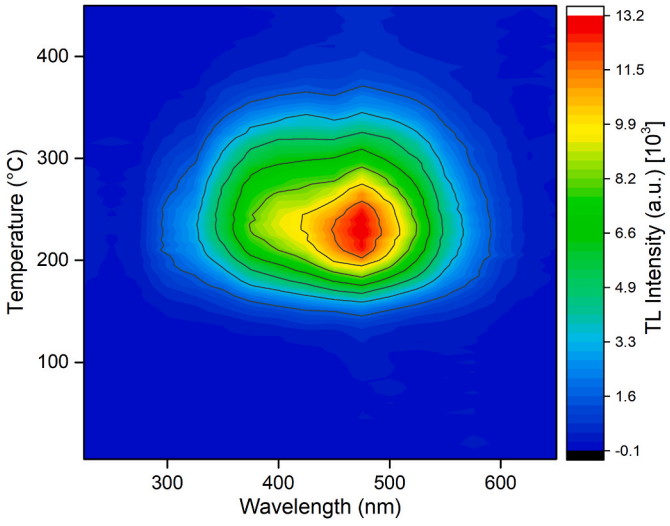

Fig. 6. 2D TL emission spectrum of the fluorapophyllite sample irradiated with a gamma dose of 1 kGy.

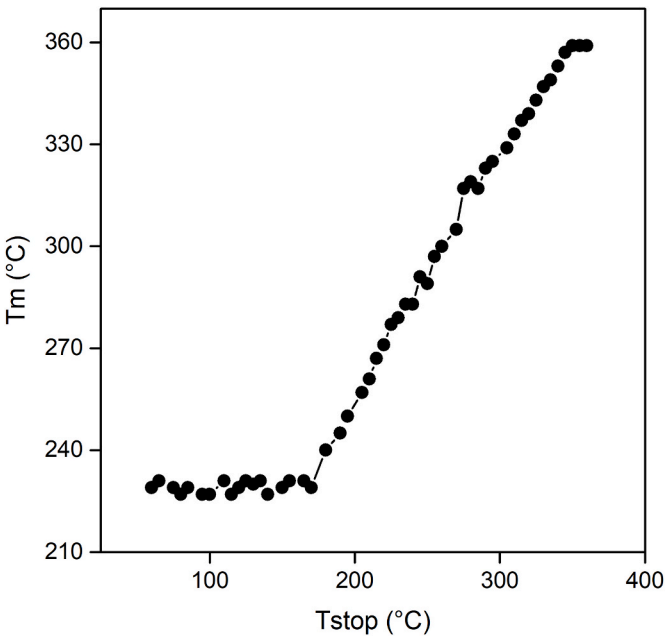

Fig. 7. Tm-Tstop plot for TL glow curve of fluorapophyllite sample irradiated with 1 kGy.

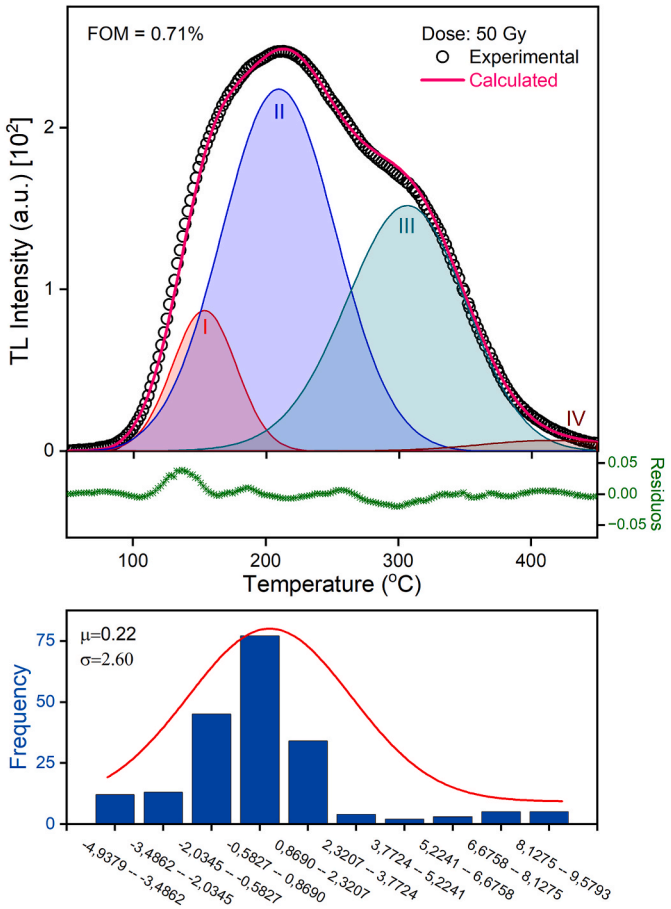

Fig. 8. (Top) Deconvolution graph of the glow curve for a sample of fluorapophyllite irradiated with a gamma dose of 50 Gy, and the residue of the deconvolution. (Bottom) Statistical analysis of the residue.

residuals and the reproducibility of the estimated scientific parameters, reflected in their low associated uncertainty. In addition, the quality of the fits is supported by the low values of the Figure of Merit (FOM) [26], all below 1.5 % and ranging from 0.45 % to 1.46 %. These thermoluminescent analyses were carried out based on TL glow curves obtained after irradiation in the range of 1 Gy–3 kGy, as shown in Table V of Annex I, which allowed for to study of the linearity of the response of each TL peak, component by component. The results of the corresponding adjustment are presented in Table 2.

Analysis of the parameters shows that most peaks exhibit sublinear behavior, given that their α values are less than one. In this regard, Peak IV (α = 0.47) shows the most pronounced deviation from linearity, while Peaks I (α = 0.67) and III (α = 0.71) exhibit moderate sublinearity. In contrast, peak II is the only exception, reaching a value of α = 1.06, which indicates slightly supralineal behavior and, therefore, a response whose magnitude increases slightly more rapidly than the administered dose.

Assuming that the probability of electron release from an electron trap, characterized by an activation energy E, defined as the energy difference between the trap level and the conduction band, at a given temperature, can be described by the expression proposed by McKeever [27]:

$$p = \nu \cdot K \cdot e^{-\frac{F}{k \cdot T}} \tag{5}$$

where ν is the vibrational state of the lattice, which has values between 10^{12} - 10^{14} s^{-1}, K is a value related to the possibility (K = 1) or not (K = 0) of transition, and F is the free Helmholtz function expressed as:

$$F = E - T \cdot \Delta S \tag{6}$$

Therefore, the release probability can be expressed as:

$$p = \nu \cdot K \cdot e^{\frac{\Delta S}{k}} \cdot e^{-\frac{E}{k \cdot T}} = s \cdot e^{-\frac{E}{k \cdot T}} \tag{7}$$

and the frequency factor is expressed as a constant of the form:

$$s = \nu \cdot K \cdot e^{\frac{\Delta S}{k}} \tag{8}$$

The electron release process corresponding to the first component is characterized by the highest entropic contribution, whereas the third component exhibits a comparatively lower degree of entropy change. This behavior can be explained by the compensation effect between the activation energy and the frequency factor: the high activation energy associated with the first component is balanced by a correspondingly high frequency factor, while in the third component the lower activation energy is accompanied by a reduced frequency factor. Nevertheless, the fitting results remain graphically consistent, as the low-temperature region shows a steep slope that correlates with high activation energy values, whereas the temperature range mainly associated with the third component corresponds to lower E values, as evidenced by the broadening of this region.

Fig. 9 shows the normalized TL intensity for a series of ten successive TL measurements of the fluorapophyllite sample, to verify the reproducibility of the TL signal centered at 225 °C. Reproducibility allows sensitivity changes to be evaluated during several reuse cycles or measurements. The measurements were performed with a sample previously heat treated at 700 °C, subjected to gamma ray irradiation cycles with a dose of 1 kGy, and TL reading. Reproducibility was evaluated using the coefficient of variation (CV), defined as:

$$CV = \frac{\delta}{\bar{I}} * 100\% \tag{9}$$

where δ represents the standard deviation and $\bar{I}$ is the average intensity of the ten measurements. The CV value was approximately 2.82 %, indicating good reproducibility, since according to Fureta [28], CV values below 5 % are considered acceptable.

Fig. 10 shows the TL signal fading characteristics of the

Table 2
Coefficient (a) and linearity factor (α) for the four TL peaks obtained by convolution of the TL glow curve for a dose range between 1 Gy and 3 kGy.

Area	a	α
Peak I	579.5	0.67
Peak II	252.6	1.06
Peak III	2097.7	0.71
Peak IV	161.4	0.47

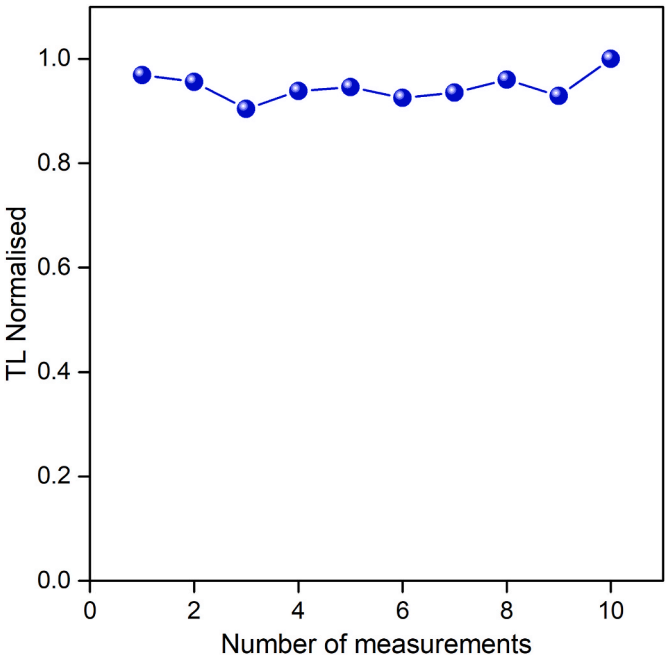

Fig. 9. Reproducibility of the TL signal from fluorapophyllite sample over ten repeated cycles of annealing-irradiation-readout.

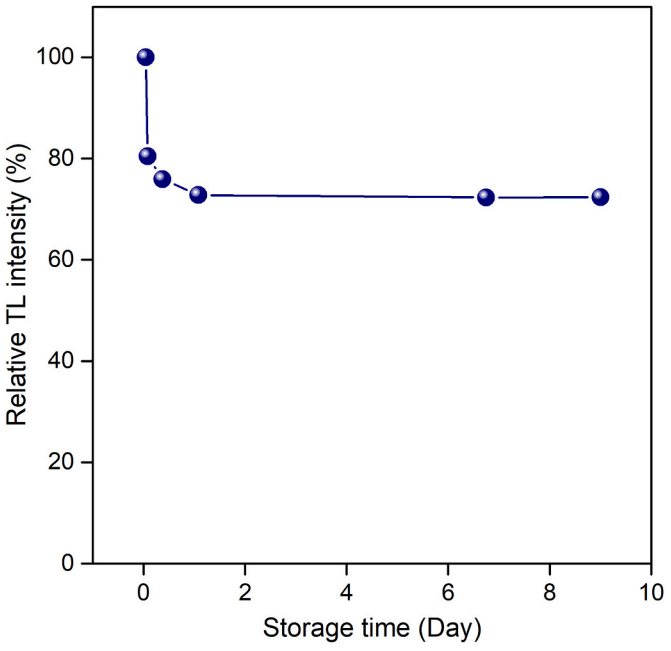

Fig. 10. Fading of the TL peak at 225 °C for the fluorapophyllite sample. Before performing the TL reading, the irradiated samples were stored in the dark at room temperature.

fluorapophyllite sample. The fading signal was obtained for the main TL peak, centered at 225 °C. The figure shows that the TL intensity decreases rapidly during the first 9 h, and then the signal decreases very slightly. After one day, the TL signal intensity had decreased by 27 %. For times longer than one day, the TL signal does not show any fading. Therefore, the TL measurements of the previously irradiated fluorapophyllite sample were performed after one day of storage.

The EPR spectroscopy technique has been used to identify the possible defect centers involved in the charge transfer mechanisms responsible for the thermoluminescent emission. The objective of this study is to correlate the TL and EPR results to identify the centers responsible for both physical properties, i.e., the centers responsible for the material's paramagnetic and luminescent properties.

Fig. 11 shows the result of the EPR measurement performed on the natural material. One center associated with the V^{4+} ion was identified, interpreted as the vanadyl ion (VO^{2+}), as described by Vassilikou-Dova and Lehmann [29]. In addition, an oxygen-associated (O^- ion) center was identified, characterized by its axial symmetry and by presenting a broad absorption line (0.4 mT). The g values determined for this center were $g_{\|} = 2.002$ and $g_{\perp} = 2.044$, which agree with the results reported by Mao and Pan [19].

To investigate the effect of heat treatment on the identified paramagnetic centers and fluorapophyllite structure, as well as to correlate them with TL and OA results, a series of successive heat treatments between 300 and 470 °C were performed on samples previously irradiated with a gamma radiation dose of 1 kGy. Fig. 12 shows the EPR spectra of some of the heat treatments. At 310 °C and above, attenuation of the oxygen-associated center (g = 2.044) was observed. This result corroborates the results obtained by AO (see Fig. 3) and the EPR results obtained by Mao and Pan [19]. The centers related to VO^{2+} and O^- ions showed a progressive reduction in intensity until they disappeared completely around 430 °C. Despite a significant decrease in the intensity of the VO^{2+} center, it remains present even at 430 °C.

The crystal structure of fluorapophyllite consists of silicate layers interconnected by Ca^{2+} and K^+ ions as well as oxygen atoms via hydrogen bonds. The silicate layers are centered at positions z = 1/4 and 3/4 and are perpendicular to the (001) plane. The K^+, Ca^{2+}, and F^- ions

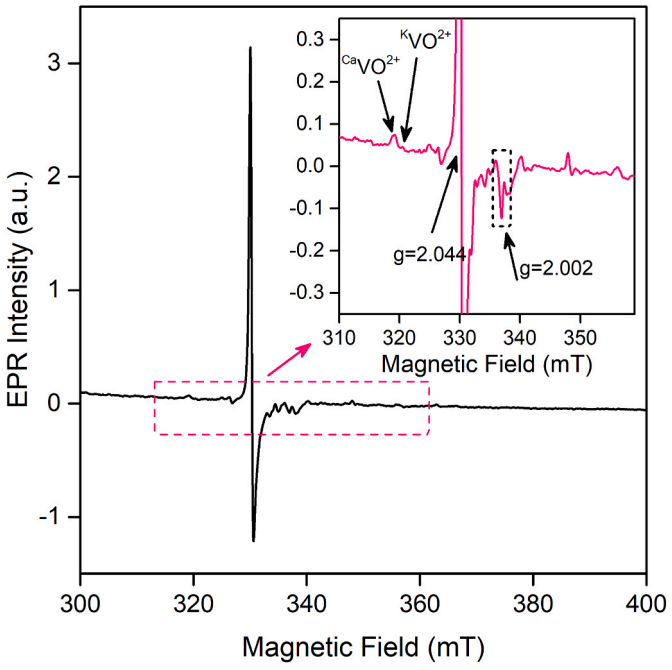

Fig. 11. EPR spectrum of the natural fluorapophyllite powder sample as received. An enlargement of the weak EPR signals is shown in the inset of the figure.

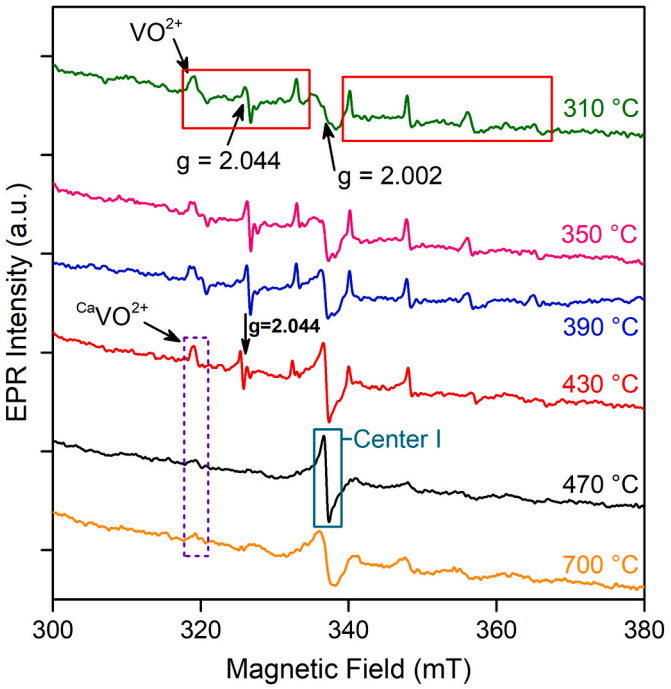

Fig. 12. EPR spectra of fluorapophyllite powder samples irradiated with a gamma dose of 1 kGy and heat treated at 310, 350, 390, 430, 470, and 700 °C.

are located in specular planes at positions z = 0 and z = 1/2. The K^+ ion coordinates eight oxygen atoms of the water molecules, while the Ca^{2+} ion coordinates four oxygen atoms of the silicate layers. The polyhedron $K^+(OH_2)_8$ is connected to the silicate layers through both direct hydrogen bonds and indirect coordination with Ca^{2+}. The water molecules in the fluorapophyllite structure, although crystallographically equivalent, have two types of interactions: a stronger H (1)-O (3) type and a weaker H (2)-O (2) type [30].

Although fluorapophyllite is not classified as a zeolite, part of the water in its composition is considered zeolitic and is trapped between the layers of the mineral, while another part is directly coordinated to the crystal structure [12,31]. The fraction of water lost in the initial stages of heating, up to about 200 °C, corresponds to water molecules in the layers of the mineral. The water loss between 200 °C and 500 °C, which directly influences the TL behavior of the mineral, is associated with crystal structure-coordinated water molecules. According to Stahl [30], the dehydration process of fluorapophyllite between 300 and 500 °C is governed by thermal diffusion and occurs in two distinct stages: the first involves the release of water molecules coordinated to the K^+ ion, and the second causes the destabilization of the coordination of K^+ and Ca^{2+} ions, resulting in the formation of an amorphous phase. Mao and Pan [19], using EPR analysis, observed that the decrease in the intensity of VO_2^+ centers at K sites between 300 and 340 °C is comparable to the results obtained by Ramakrishnan et al. [32] after heat treatment of apophyllite crystals at 230 °C. Around 430 °C, the disappearance of the signal associated with the VO_2^+ center indicates the collapse of the sites occupied by the vanadyl ion, suggesting the transition to an amorphous phase [19,30,33]. These observations are corroborated by Marriner et al. [20], who, using differential thermal analysis (DTA), identified two dehydration bands related to water molecules coordinated to the cations in fluorapophyllite: the first between 310 and 340 °C, and the second between 430 and 450 °C. From these results, we can infer that the TL emission observed in fluorapophyllite up to a temperature of 500 °C is not exclusively related to dehydration but rather to the nature of the water present in the crystal structure.

Mao and Pan [19] report that eight water molecules are exhaled in the first stage of the dehydration process, suggesting the onset of a

permanent amorphous phase after the second stage. On the other hand, Marriner et al. [20], who used DTA analysis, found that only five water molecules are released in the first stage, corresponding to approximately 10 % of the total mass. The remaining three molecules are released in the second stage, when the crystal lattice is destabilized and the amorphous phase begins to form. However, most of the crystal structure is preserved, which is attributed to the presence of fluorine, an essential element for the structural integrity of the system. Thus, the higher the fluorine content, the higher the resistance of fluorapophyllite to structural fragmentation at high temperatures. According to Marriner et al. [20], no significant loss of fluorine was detected up to around 460 °C. However, at temperatures around 800 °C, a loss of approximately 1 % of the fluorine content was observed, a value that may vary depending on the applied heating rate; the higher the rate, the greater the loss. Complete fluorine removal was observed at 930 °C. Considering that the release of water molecules coordinated to cations occurs between 430 and 450 °C, as indicated by Marriner et al. [20], it can be inferred that dehydration is not the determining factor for the appearance of the amorphous phase, which is only observed around 600 °C. Fluorapophyllite dehydrates completely at 600 °C and initiates the formation of an amorphous phase that persists until shortly after 700 °C. From about 780 °C, a significant loss of fluorine is observed, which substantially compromises the structural integrity of the mineral, a fact that justifies the decrease in the intensity of the TL signal from this temperature onwards. This process culminates, at around 860 °C, with the transformation of fluorapophyllite to wollastonite-β and subsequently to wollastonite-α at a temperature of around 1100 °C [20].

Fig. 12 shows the EPR spectra of fluorapophyllite irradiated with 1 kGy and subjected to heat treatments up to 700 °C. The importance of calcium in maintaining the fluorapophyllite structure lies in the fact that it simultaneously coordinates four oxygen atoms of the silicate layers and four fluorine atoms. The persistence of the VO^{2+} center, albeit to a lesser extent, together with the stability of the center labeled as I in Fig. 12 (g = 2.002) between 470 and 700 °C, suggests that most of the basic crystal structure is maintained, although not necessarily its crystallographic planes. The stability of the O^- center remains constant in the samples analyzed at room temperature (no heat treatment) and up to about 200 °C. From this point, there is a sharp drop in its intensity, which reaches zero at around 470 °C (see Fig. 13). As for the signal at g = 2.002, it is observed that this center presents low intensity and relative stability up to approximately 220 °C. However, from this temperature onwards, there is an unstable increase in signal intensity, which lasts up to 470 °C. From this level, the intensity begins to grow continuously until it reaches its maximum value at 700 °C, at which point a process of decrease begins with increasing temperature.

Variations in the intensity and stability of the O^- centers are the result of irradiation, which favors the appearance and growth of these centers. However, the increase in temperature is closely related to the dehydration process of the crystal. In this context, it is observed that the signal intensity at g = 2.002 increases, while the O^- ion intensity decreases. These results suggest that the O^- ion originates from the ionization of hydroxyl groups (OH^-) located at sites with coordinates z = 0 and z = ½. As these groups volatilize, there is an immediate and instantaneous reduction in the intensity of the associated center.

The center, due to the O^- ion corresponds to the main TL peak of the fluorapophyllite sample. This center is formed when oxygen captures a positively charged hole, thus creating a TL center that acts as an electron capture trap. Due to the structural configuration of the crystal, as long as water is present in the lattice, radiation-induced paramagnetic centers are more likely to form from OH groups than their silicate-related counterpart. This difference explains the intensity variation observed in the EPR spectra, associated with the presence of water in the crystal structure. However, this dynamic changes with heat treatment: the reduction in water content causes the progressive elimination of centers related to OH groups and increases the formation of center I from the silicate. This increase is not only due to the absence of H_2O, but also to the increased availability of positive lattice voids, which are created both by water loss and thermodynamic diffusion of these defects. As a result, after heat treatment at 700 °C, a single center (center I) predominates, detectable by EPR with a signal at $g = 2.002$ (see Fig. 14).

Center I (Fig. 12) displays an isotropic EPR line with a g-value of 2.002 and a linewidth of approximately 7 G. Irradiation can lead to the formation of F centers (or F^+ centers in oxides), where electrons become

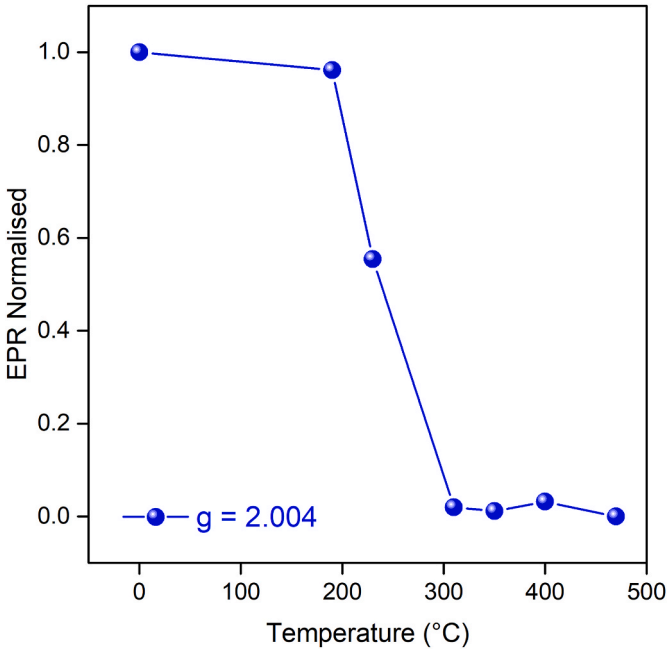

Fig. 13. EPR signal intensity behavior of the O^- ion ($g_\perp = 2.044$ component) as a function of heat treatment.

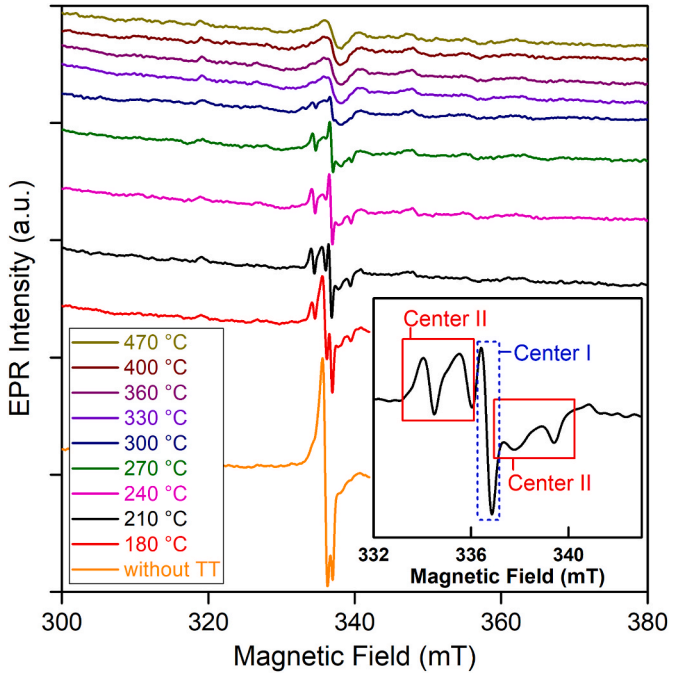

Fig. 14. EPR spectra for different heat treatments of fluorapophyllite samples, which were previously annealed at 700 °C and irradiated with 1 kGy. The inset of the figure shows an enlargement of the EPR spectrum of the sample after heat treatment at 210 °C (black line), along with the identification of the defect centers responsible for the EPR signals.

trapped at anion vacancies. This phenomenon is well known in materials such as alkali halides, alkaline-earth halides, and various oxides. Early studies by Hutchinson [34] reported broad F-center linewidths of approximately 100 G in alkali halides. In contrast, the intrinsic linewidth in MgO is much narrower, around 1 G [35]. The linewidth is influenced by the degree of electron delocalization and interactions with nearby ions, as well as factors such as isotopic composition and the magnetic moments of surrounding atoms. For example, F center linewidths in KCl and LiCl are reported to be approximately 20 G and 58 G, respectively [36].

During irradiation, an anion vacancy can trap an electron, forming an F center that may exhibit either a positive or negative *g*-shift. The *g*-value of such centers generally remains close to the free-electron value of 2.0023. In fluorapophyllite, Center I is observed with a *g*-value of 2.002 and a linewidth of 7 G. Given these characteristics and the known behavior of F centers (or F^+ centers in oxides), Center I is tentatively assigned to an F^+ center.

The sample, previously treated at 700 °C and irradiated with 1 kGy and heat treated at 210 °C before EPR spectrum measurement (see inset of Fig. 14), clearly shows EPR signals from a center that exhibits an axial *g*-tensor with principal values $g_{\parallel} = 2.0$ and $g_{\perp} = 2.020$. The center displays hyperfine splitting arising from the interaction of the unpaired spin with a spin ½ nucleus. The doublets seen in the inset of Fig. 14 are the result of this interaction. The hyperfine splitting is estimated to be about 16 G.

One of the likely defect center that can form in the present system is the O^- ion, which is a positive hole localized on an oxygen ion near a cation vacancy. Cation vacancies provide the stability of the hole through electrostatic attraction. The hole resides in an oxygen *p*-orbital in an O^- ion and exhibits positive *g*-shifts. Based on the relatively large *g*-shift, center II is tentatively identified as the O^- ion.

Previous studies have demonstrated that O^- hole centers can exhibit hyperfine interactions with nearby ions. For example, in $LiNbO_3$, the O^- ion interacts with three neighboring ions. In Li_3VO_4, Murata and Miki [37] reported a hyperfine interaction between an O^- ion and a neighboring vanadium ion, as each oxygen ion in that system has one nearest-neighbour vanadium atom. By analogy, the hole localized on an oxygen ion in fluorapophyllite may also interact with a nearby ion, giving rise to similar hyperfine features.

4. Conclusions

XRD analysis confirmed the crystalline structure of fluorapophyllite, and elemental analyses by XRF and EDS confirmed the presence of the constituent elements of this crystal. Four optical absorption bands associated with O-H + H_2O, NH_2, H_2O, and OH molecules were found. Fluorapophyllite sensitized by heat treatment at 700 °C showed four TL emission peaks at 172, 230, 306, and 413 °C, which overlap to form a very broad TL peak centered at approximately 225 °C, and an emission band between 300 and 600 nm centered at 475 nm. The broad peak centered at 225 °C increases linearly with the gamma radiation dose in the range of 50 Gy to 3 kGy. EPR analysis of γ-irradiated fluorapophyllite reveals two primary defect centers: a VO^{2+} center and an O^- ion. The O^- center is closely associated with the main TL peak at 230 °C. Upon thermal annealing, two more centers (centers I and II) become apparent. The thermal evolution of the sample indicates a transition in the origin of the TL centers, initially associated with OH-groups, and later with the oxygens of the silicate network, as a result of the dehydration process. The structural stability observed up to 700 °C reinforces the potential of fluorapophyllite as a sensitive material for radiation dosimetry applications.

CRediT authorship contribution statement

Reinaldo de Melo Ferreira: Writing – original draft, Resources, Investigation, Formal analysis, Data curation, Conceptualization. **Nilo F. Cano:** Writing – original draft, Validation, Software, Investigation, Formal analysis, Conceptualization, Writing – review & editing, Visualization. **Betzabel N. Silva-Carrera:** Writing – original draft, Investigation, Formal analysis. **T.K. Gundu Rao:** Writing – original draft, Validation, Supervision, Investigation, Formal analysis, Writing – review & editing. **J.F. Benavente:** Writing – original draft, Visualization, Validation, Software, Formal analysis, Data curation, Writing – review & editing. **Edwar A. Canaza:** Software, Methodology, Formal analysis. **Jessica Mosqueira-Yauri:** Methodology, Investigation, Formal analysis. **René R. Rocca:** Methodology. **J.F.D. Chubaci:** Visualization, Validation, Supervision, Conceptualization.

Declaration of competing interest

The authors declare that they have no known competing financial interests or personal relationships that could have appeared to influence the work reported in this paper.

Acknowledgements

The authors would like to express thanks to Ms. E. Somessari from the Institute for Energy and Nuclear Researches (IPEN/CNEN-SP), Brazil, for kindly carrying out the γ-irradiation of the samples.

Appendix A. Supplementary data

Supplementary data to this article can be found online at https://doi.org/10.1016/j.jlumin.2025.121631.

Data availability

Data will be made available on request.

References

[1] K. Wedepohl, Geochemistry, Holt, Rinehart & Winston, New York, 1971.
[2] Q.D. Truong, M.K. Devaraju, T. Tomai, I. Honma, Direct observation of antisite defects in LiCoPO4 cathode materials by annular Dark- and bright-field electron microscopy, ACS Appl. Mater. Interfaces 5 (2013) 9926, https://doi.org/10.1021/am403018n.
[3] M.M. Kuklja, Defects in yttrium aluminium perovskite and garnet crystals: atomistic study, J. Phys. Condens. Matter 12 (2000) 2953, https://doi.org/10.1088/0953-8984/12/13/307.
[4] A.P. Patel, M.R. Levy, R.W. Grimes, R.M. Gaume, R.S. Frigelson, K.J. McClellan, C. R. Stanek, Mechanisms of nonstoichiometry in $Y_3Al_5O_{12}$, Appl. Phys. Lett. 93 (2008) 191902.
[5] J.A.H. Lucas, Espèce Apophyllite, in: Tableau Méthodique Des Espèces Minérales, Première Partie, Chez Levrault, 1806, pp. 266–268. Paris.
[6] P.J. Dunn, W.E. Wilson, Nomenclature revisions in the apophyllite group: hydroxyapophyllite apophyllite fluorapophyllite, Mineral. Rec. 9 (1978) 95–98.
[7] H. Matsueda, Y. Miura, J. Rucklidge, Natroapophyllite, a new orthorhombic sodium analog of apophyllite I. Description, occurrence, and nomenclature, Am. Mineral. 66 (1981) 410–415.
[8] F. Hatert, S.J. Mills, M. Pasero, P.A. Williams, CNMNC guidelines for the use of suffixes and prefixes in mineral nomenclature, and for the preservation of historical names, Eur. J. Mineral 25 (2013) 113–115, https://doi.org/10.1127/0935-1221/2013/0025-2267.
[9] E.A. Burke, Tidying up mineral names: an IMA-CNMNC scheme for suffixes, hyphens and diacritical marks, Mineral. Rec. 39 (2008) 131–135.
[10] Y.V. Seryotkin, M.A. Ignatov, Structure evolution of fluorapophyllite-(K) under high pressure, High Press. Res. 43 (2023) 279–292, https://doi.org/10.1080/08957959.2023.2248357.
[11] Ş. Marincea, D.G. Dumitraş, C.S. Ghineţ, A.E. Filiuţă, F.D. Bo, F. Hatert, G. Costin, Ammonium-Bearing Fluorapophyllite-(K) in the Magnesian Skarns from Aleului Valley, vol. 13, 2023, p. 1362, https://doi.org/10.3390/min13111362. Pietroasa, Romania, Miner.
[12] F.V. Chukhrov, L.P. Yermilova, L.L. Shanin, The age problem of apophyllite in late hydrothermal mineral associations, Int. Geol. Rev. 16 (1974) 417–426, https://doi.org/10.1080/00206817409471853.
[13] N.F. Cano, A.R. Blak, S. Watanabe, Correlation between electron paramagnetic resonance and thermoluminescence in natural sodalite, Phys. Chem. Miner. 37 (2010) 57–64, https://doi.org/10.1007/s00269-009-0309-z.
[14] N.F. Cano, L.H.E. dos Santos, J.F.D. Chubaci, S. Watanabe, Study of luminescence, color and paramagnetic centers properties of albite, Spectrochim. Acta 137 (2015) 471–476, https://doi.org/10.1016/j.saa.2014.08.085.

[15] N.F. Cano, A.R. Blak, J.S. Ayala-Arenas, S. Watanabe, Mechanisms of TL for production of the 230°C peak in natural sodalite, J. Lumin. 131 (2011) 165–168, https://doi.org/10.1016/j.jlumin.2010.09.027.
[16] M. Gaft, R. Reisfeld, G. Panczer, Modern Luminescence Spectroscopy of Minerals and Materials, Springer, 2015.
[17] J.F. Benavente, J.M. Gómez-Ros, A.M. Romero, Thermoluminescence glow curve deconvolution for discrete and continuous trap distributions, Appl. Radiat. Isot. 153 (2019) 108843, https://doi.org/10.1016/j.apradiso.2019.108843.
[18] A. Dumas, M. Mizrahi, F. Martin, F.G. Requejo, Local and extended-order evolution of synthetic talc during hydrothermal synthesis: extended X-ray absorption fine structure, X-ray diffraction, and fourier transform infrared spectroscopy studies, Cryst. Growth Des. 15 (2015) 5451–5463, https://doi.org/10.1021/acs.cgd.5b01076.
[19] M. Mao, Y. Pan, Radiation-induced defects in apophyllites. I. The NH2 free radical in fluorapophyllite, Eur. J. Mineral 21 (2009) 317–324, https://doi.org/10.1127/0935-1221/2009/0021-1902.
[20] G.F. Marriner, J. Tarney, J.I. Langford, Apophyllite group: effects of chemical substitutions on dehydration behaviour, recrystallization products and cell parameters, Mineral. Mag. 54 (1990) 567–577, https://doi.org/10.1180/minmag.1990.054.377.06.
[21] N. Kristianpoller, R. Chen, M. Israeli, Dose dependence of thermoluminescence peaks, J. Phys. D Appl. Phys. 7 (1974) 1063, https://doi.org/10.1088/0022-3727/7/7/313.
[22] V. Pagonis, G. Kitis, Prevalence of first-order kinetics in thermoluminescence materials: an explanation based on multiple competition processes, Phys. Status Solidi B 249 (2012) 1590–1601, https://doi.org/10.1002/pssb.201248082.
[23] A. Halperin, R. Chen, Thermoluminescence of semiconducting diamonds, Phys. Rev. 148 (1966) 839–845, https://doi.org/10.1103/PhysRev.148.839.
[24] S.W.S. McKeever, Thermoluminescence of Solids, Cambridge University Press Cambridge, 1985.
[25] E.J. Pilco, N.F. Cano, J.S. Ayala-Arenas, J.A. Suárez-Navarro, J.F. Benavente, Numerical studies to validate mathematical models based on first-order and general-order kinetic approaches for fitting TL glow curves, Phys. Lett. 553 (2025) 130674, https://doi.org/10.1016/j.physleta.2025.130674.
[26] H.G. Balian, N.W. Eddy, Figure-of-merit (FOM), an improved criterion over the normalized chi-squared test for assessing goodness-of-fit of gamma-ray spectral peaks, Nucl. Instrum. Methods 145 (1977) 389–395, https://doi.org/10.1016/0029-554X(77)90437-2.
[27] S.W.S. McKeever, A Course in Luminescence Measurements and Analyses for Radiation Dosimetry, John Wiley & Sons, 2022.
[28] C. Furetta, Handbook of Thermoluminescence, World Scientific Publishing Co. Pte. Ltd, 2003, https://doi.org/10.1142/5167.
[29] A.B. Vassilikou-Dova, G. Lehmann, EPR of V^{4+} in apophyllite, Phys. Status Solidi (b) 147 (1988) 691–697, https://doi.org/10.1002/pssb.2221470228.
[30] K. Stahl, A neutron powder diffraction study of partially dehydrated fluorapophyllite, $KCa_4Si_8O_{20}F.6.9H_2O$, Eur. J. Mineral 5 (1993) 845–849.
[31] R.L. Frost, Z. Ding, J.T. Kloprogge, The application of near-infrared spectroscopy to the study of brucite and hydrotalcite structure, Can. J. Anal. Sci. Spectrosc. 45 (2000) 96–101.
[32] G. Ramakrishnan, M.B.V.L.N. Swamy, P.S. Rao, S. Subramanian, EPR of vanadyl ion in a natural mineral, apophyllite, Proc. Indian Acad. Sci. 103 (1991) 613–619, https://doi.org/10.1007/BF02841062.
[33] R. Wlodyka, Raman spectroscopic study of the dehydration behavior in fluorapophyllite, Polsk. Towarz. Mineral 20 (2002) 228–230.
[34] C.A. Hutchison, Paramagnetic resonance absorption in crystals colored by irradiation, Phys. Rev. 75 (1949) 1769–1770, https://doi.org/10.1103/PhysRev.75.1769.2.
[35] J.E. Wertz, P. Auzins, R.A. Weeks, R.H. Silsbee, Centers in magnesium oxide; confirmation of the spin of magnesium-25, Phys. Rev. 107 (1957) 1535–1537, https://doi.org/10.1103/PhysRev.107.1535.
[36] W.C. Holton, H. Blum, Paramagnetic resonance of F centers in alkali halide, Phys. Rev. 125 (1962) 89–103, https://doi.org/10.1103/PhysRev.125.89.
[37] T. Murata, T. Miki, Trapped-hole centers in irradiated Li3VO4, J. Appl. Phys. 73 (1993) 1110–1113, https://doi.org/10.1063/1.353274.